Research Article Vol. 3, No. 1 / January 2016 / Optica 75

Scale-invariant nonlinear optics in gases

C. M. Heyl,[1,*] H. Coudert-Alteirac,[1] M. Miranda,[1] M. Louisy,[1] K. Kovacs,[2,3] V. Tosa,[2,3] E. Balogh,[3,4] K. Varjú,[3,4] A. L'Huillier,[1] A. Couairon,[5] and C. L. Arnold[1]

[1]Department of Physics, Lund University, P. O. Box 118, SE-221 00 Lund, Sweden
[2]National Institute for R&D Isotopic and Molecular Technologies, Cluj-Napoca, Romania
[3]ELI-ALPS, ELI-Hu Nkft, Dugonics ter 13, Szeged 6720, Hungary
[4]Department of Optics and Quantum Electronics, University of Szeged, Dom ter 9, 6720 Szeged, Hungary
[5]Centre de Physique Théorique, École Polytechnique, CNRS, F-91128 Palaiseau, France
*Corresponding author: christoph.heyl@fysik.lth.se

Received 5 November 2015; revised 8 December 2015; accepted 9 December 2015 (Doc. ID 253362); published 13 January 2016

Nonlinear optical methods have become ubiquitous in many scientific areas, from fundamental studies of time-resolved electron dynamics to microscopy and spectroscopy applications. They are, however, often limited to a certain range of parameters such as pulse energy and average power. Restrictions arise from, for example, the required field intensity as well as from parasitic nonlinear effects and saturation mechanisms. Here, we identify a fundamental principle of nonlinear light–matter interaction in gases and show that paraxial nonlinear wave equations are scale-invariant if spatial dimensions, gas density, and laser pulse energy are scaled appropriately. As an example, we apply this principle to high-order harmonic generation and provide a general method for increasing peak and average power of attosecond sources. In addition, we experimentally demonstrate the implications for the compression of short laser pulses. Our scaling principle extends well beyond those examples and includes many nonlinear processes with applications in different areas of science.

OCIS codes: (190.0190) Nonlinear optics; (070.7345) Wave propagation; (320.7110) Ultrafast nonlinear optics; (190.2620) Harmonic generation and mixing.

http://dx.doi.org/10.1364/OPTICA.3.000075

1. INTRODUCTION

The field of nonlinear optics started directly after the invention of the laser with the demonstration of frequency doubling in quartz in 1961 [1]. Rapidly, it became essential in many scientific areas, exploiting optical nonlinearities in a variety of media ranging from crystals and fibers to liquids and gases [2]. Today, nonlinear interactions of intense short laser pulses with gaseous media form the basis behind a wealth of interesting phenomena such as multiphoton ionization [3] and plasma formation [4], spectral broadening (which can be used for pulse compression [5–7]), harmonic generation and wave mixing [8], as well as the creation of attosecond pulses [9] and the formation of electron or ion beams [10]. An essential foundation of nonlinear optics is the understanding of nonlinear wave propagation. Today, nonlinear wave equations, which can be directly derived from Maxwell's equations, are routinely used to describe the propagation of ultrashort laser pulses and their linear and nonlinear interactions with matter. These wave equations allow us to model even highly complex wave propagation phenomena, such as filamentation [11] or the guiding of few-cycle pulses in photonic crystal fibers [12]. This is important for understanding experimental measurements and for finding optimum conditions, e.g., the laser power for maximizing the desired output of a secondary radiation process or the best geometry for phase-matched wave mixing.

While optimum conditions are often well explored experimentally within rather narrow parameter ranges, the rapid advances in femtosecond laser technology, driven by the desire to access, e.g., faster times scales or to reach higher intensities [13–15], demand the extension of nonlinear optical methods to unexplored parameter regimes. However, to date, no general methodology that allows transforming nonlinear optics phenomena into new parameter regimes while preserving the essential characteristics of the nonlinear processes involved has been put forward.

Here we present such a methodology and introduce a set of general scaling laws for nonlinear light–matter interactions, directly derived from basic paraxial propagation equations for ultrashort laser pulses. We identify a fundamental principle of nonlinear optics showing that even highly complex nonlinear propagation phenomena in gases are scale-invariant, if appropriate scaling relations are employed. We apply our model to two important examples of modern photonics, filamentation in gases used, e.g., for laser pulse compression, and high-order harmonic generation (HHG), which provides the basis for attosecond science. We show how these processes can be invariantly scaled to laser pulse energies well above the 100 mJ level, with no fundamental upper limit, and discuss the limitations arising at small pulse energies. Moreover, we experimentally verify the invariant scalability of pulse compression via filamentation within a driving

laser pulse energy range exceeding 1 order of magnitude. Our scaling formalism is simple and general, and opens up completely new parameter regimes for nonlinear optics in gaseous media and, more generally, for ultrafast science.

2. SCALING PRINCIPLES

We illustrate our scale-invariant nonlinear optics framework using general wave equations. Nonlinear pulse propagation in gases (including generation of new frequencies) is usually treated using wave equations in scalar and paraxial approximation, which can be directly derived from Maxwell's equations. Such wave equations describe electromagnetic waves propagating in one direction, exhibiting only small angles relative to the optical axis. Without any limitation of the spectral bandwidth and thus of the minimum pulse duration, the propagation equation for the electrical field in frequency representation $\hat{E}(r,z,\omega)=\int_{-\infty}^{\infty}\exp(i\omega t)E(r,z,t)\mathrm{d}t$, usually referred to as the forward Maxwell equation [16], can be written as

$$\left[\frac{\partial}{\partial z}-\frac{i}{2k(\omega,\rho)}\Delta_\perp-ik(\omega,\rho)\right]\hat{E}=\frac{i\omega^2}{2k(\omega,\rho)c^2\varepsilon_0}\hat{P}_{\mathrm{NL}}. \quad (1)$$

Here, $k(\omega,\rho)=n(\omega,\rho)\omega/c$ denotes the wave number with angular frequency ω, refractive index $n=n(\omega,\rho)$, and c is the speed of light in vacuum. ρ is the gas density, $\hat{P}_{\mathrm{NL}}$ is the frequency representation of the nonlinear polarization induced by the electric field E, and ε_0 is the vacuum permittivity. For short pulse propagation, exact knowledge of the refractive index n, e.g., in the form of a Sellmeier equation, is required. For pulse propagation in the visible and near-infrared spectral region, $k(\omega,\rho)$ is usually real-valued, but linear absorption can easily be included by a complex wave number. For the sake of simplicity, we consider linear polarization and rotational symmetry and, thus, a single radial coordinate r, although our formalism does not require these simplifications. The transverse Laplace operator in Eq. (1) then becomes $\Delta_\perp=\partial^2/\partial r^2+1/r\cdot\partial/\partial r$. Via the nonlinear polarization, a large number of nonlinear interactions can be considered, such as self-focusing, self-phase modulation, field ionization, harmonic generation, and plasma defocusing.

For propagation in vacuum, the right-hand side of Eq. (1) vanishes and $k(\omega,\rho)\to k(\omega,0)=\omega/c$. We now introduce the field $\hat{\mathcal{E}}\equiv\hat{E}\exp[-i\omega z/c]$ and rewrite Eq. (1):

$$\left[\frac{\partial}{\partial z}-\frac{ic}{2\omega}\Delta_\perp\right]\hat{\mathcal{E}}=0. \quad (2)$$

The change of fields from $\hat{E}$ to $\hat{\mathcal{E}}$ formally corresponds to a transformation of Eq. (1) from the laboratory frame to a frame moving at the vacuum speed of light c [17]. It should be noted that $\hat{\mathcal{E}}$ is an electric field, not an envelope. No envelope approximations and thus no restrictions on the spectral bandwidth are made. Equation (2) is invariant under the following transformations: $r\to\eta r$ and $z\to\eta^2 z$ (see Table 1), where η is a scaling parameter. If $\hat{\mathcal{E}}(r,z)$ is a solution to the wave equation, $\hat{\mathcal{E}}(r/\eta,z/\eta^2)$ is a solution, as well. For monochromatic waves, one prominent solution of Eq. (2) is the Gaussian beam. The scaling is obvious for the characteristic spatial parameters of the Gaussian beam, i.e., the beam radius W_0 and the Rayleigh length z_{R}: $W_0\to\eta W_0$ and $z_{\mathrm{R}}\to\eta^2 z_{\mathrm{R}}$. While the Gaussian beam is just one possible solution to Eq. (2), more generally, any kind of beam that can be described by this wave equation is scale-invariant under the above specified transformation.

Table 1. Scaling Relations Derived in This Work[a]

	Parameter	Scaled Parameter
Input Parameters		
Dimensions	z	$\eta^2 z$
	r	ηr
Other parameters	ρ	ρ/η^2
	$\varepsilon_{\mathrm{in}}$	$\eta^2\varepsilon_{\mathrm{in}}$
Output Parameters		
General	$\varepsilon_{\mathrm{out}}$	$\eta^2\varepsilon_{\mathrm{out}}$
Filamentation	p_{cr}	$\eta^2 p_{\mathrm{cr}}$
	z_{cr}	$\eta^2 z_{\mathrm{cr}}$
HHG	ε_q	$\eta^2\varepsilon_q$
	Γ_q	Γ_q

[a] p_{cr} and z_{cr} denote the critical power and the distance, respectively, at which an initially collimated beam collapses due to self-focusing. ε_q and Γ_q, respectively, denote the harmonic pulse energy and the conversion efficiency into harmonic order q.

These basic scaling principles can be generalized to ultrashort laser pulse propagation in gases and a wide range of nonlinear interactions, if the medium density and the input laser pulse energy $\varepsilon_{\mathrm{in}}$ are included as scaling parameters. By introducing $\hat{\mathcal{E}}$ and $\hat{\mathcal{P}}_{\mathrm{NL}}\equiv\hat{P}_{\mathrm{NL}}\exp[-i\omega z/c]$ into Eq. (1), we obtain

$$\left[\frac{\partial}{\partial z}-\frac{i}{2k(\omega,\rho)}\Delta_\perp-iK(\omega,\rho)\right]\hat{\mathcal{E}}=\frac{i\omega^2}{2k(\omega,\rho)c^2\varepsilon_0}\hat{\mathcal{P}}_{\mathrm{NL}}(\rho), \quad (3)$$

where $K(\omega,\rho)=k(\omega,\rho)-k(\omega,0)$ is proportional to ρ and describes pulse dispersion (see Supplement 1). By neglecting the weak pressure dependence of $k(\omega,\rho)$ in the denominator of the diffraction term, the left-hand side of Eq. (3) is invariant under the above transverse and longitudinal scaling transformations, if simultaneously the gas density is scaled, i.e., $\rho\to\rho/\eta^2$. Similarly, the nonlinear polarization and, consequently, the right-hand side of Eq. (3) are proportional to gas pressure p for a wide range of nonlinear interactions (throughout the paper, we assume $p\propto\rho$, taking into account a constant temperature). Finally, the input energy $\varepsilon_{\mathrm{in}}$, proportional to the radial (and temporal) integral of the absolute square of the input field, needs to be scaled as $\varepsilon_{\mathrm{in}}\to\eta^2\varepsilon_{\mathrm{in}}$, to ensure that the field amplitude, which affects $\hat{\mathcal{P}}_{\mathrm{NL}}$, is kept constant under the scaling transformation. The output pulse energy $\varepsilon_{\mathrm{out}}$, proportional to the integral of the absolute square of the field at the end of the medium, follows the same scaling: $\varepsilon_{\mathrm{out}}\to\eta^2\varepsilon_{\mathrm{out}}$. This scaling applies, as well, to the generation of new frequencies, as shown for the case of HHG below. In practice, geometrical scaling can be achieved by changing the focusing geometry (focal length and/or beam diameter before focusing) as well as the medium length. It should be noted that the transformation to the moving frame, leading to Eq. (3), was performed to illustrate the scaling principles, but does not constitute a general limitation of the formalism. The scaling itself is independent from the reference frame.

According to the above relations (see also Table 1), any spatiotemporal modifications of the field induced by diffraction, dispersion, or a nonlinear process that is proportional to pressure are scale invariant. In practice, an optical process in a gas medium, defined by a nonlinear effect and certain input parameters (pulse energy, gas pressure, focusing geometry), can be up- or downscaled to different pulse energies without changing its general characteristics. Furthermore, our scaling formalism preserves the carrier-envelope phase (CEP), which changes only because of

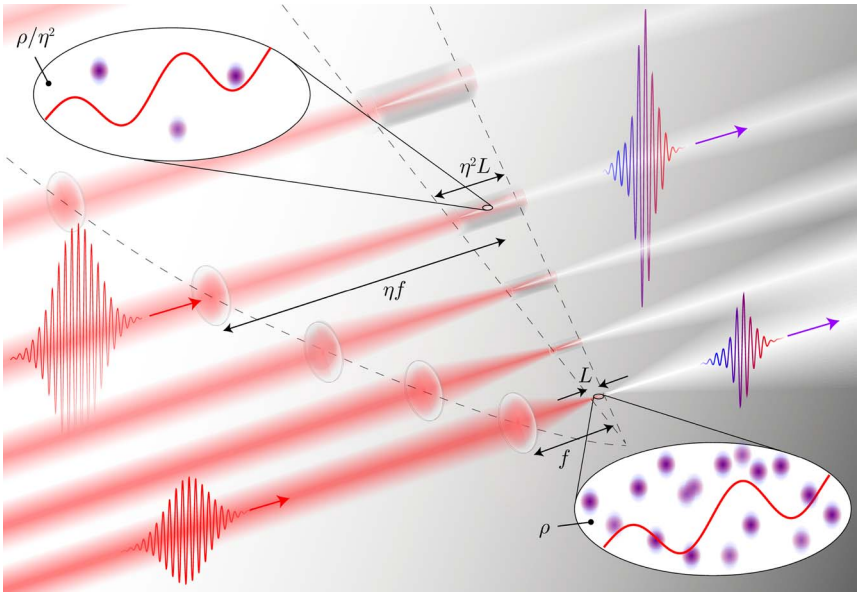

Fig. 1. Illustration of scale-invariant nonlinear optics: a laser pulse is focused (with focal length f) into a gas medium with length L and density ρ. Nonlinear propagation effects lead to a modification of the spatiotemporal pulse profile. Identical spatiotemporal modifications can be expected if a more intense laser pulse is focused more weakly (with $f \to \eta f$ to reach the same intensity) into a larger medium with length $\eta^2 L$ and lower density ρ/η^2. Note that the beam diameter before focusing is kept constant in this illustration.

linear and nonlinear (e.g., self-phase modulation) propagation effects, both of which are scale invariant. This implies that strongly CEP-dependent processes such as single attosecond pulse generation can be invariantly scaled. The scaling principle is illustrated in Fig. 1 using the example of temporal reshaping under the influence of nonlinear propagation, and is applied below to filamentation and attosecond pulse generation.

3. SCALING FILAMENTATION

A prominent example in which several nonlinear propagation effects play a critical role is filamentation [18] that occurs when self-focusing due to the Kerr effect balances defocusing caused by diffraction and plasma generation. In addition, self-phase modulation and self-compression may take place, resulting, possibly after further compression, in ultrashort pulses close to the fundamental limit of a single cycle [19]. Forming a filament requires a certain power, known as the critical power for self-focusing [20,21]. At slightly higher power, limitations arise and multiple filaments are created [22]. Different approaches were suggested to increase the output energy [19,23–27]. However, pulse compression using filaments (or similarly hollow fibers) is still limited to pulse energies of typically a few millijoules [28,29], which is approximately 2 to 3 orders of magnitude below the maximum pulse energies available from today's femtosecond laser sources.

The validity of our scaling model for filamentation can be illustrated by looking at the scaling of characteristic parameters for filamentation. The critical power for self-focusing is given by $p_{cr} = N_{cr}\lambda^2/4\pi n_0 n_2$. Here, N_{cr} is a constant depending on the spatial beam shape ($N_{cr} = 1.896$ for a Gaussian transverse profile [21]), λ is the laser wavelength, n_0 the refractive index at the central frequency, and n_2 the nonlinear refractive index. Since n_2 is, to very good approximation, proportional to the gas density, $p_{cr} \to \eta^2 p_{cr}$, thus following the same scaling relation as ε_{in}, i.e., the critical power increases linearly with laser pulse energy. It can also be shown that the distance z_{cr} at which an initially collimated laser beam collapses due to self-focusing, scales quadratically with the initial beam size (i.e., $z_{cr} \to \eta^2 z_{cr}$) [20], confirming that the scaling transformations remain valid under nonlinear propagation conditions.

We performed a more rigorous verification of our scaling model by numerically simulating filamentation with a state-of-the-art pulse propagation code (see Supplement 1). Figures 2(a) and 2(b) illustrate filamentation in Ar, using a 20 fs input pulse centered at 800 nm and two different parameter sets, where parameter set (b) corresponds to the up-scaled parameters ($\eta = 8$) of parameter set (a). In Figs. 2(a) and 2(b), the spatiotemporal intensity distribution is shown for three positions along the optical axis. In both cases, typical filamentation characteristics like conical emission and temporal self-compression [18] can be observed. Despite the very different pulse energies [$\eta^2 = 64$ times larger for parameter set (b)] and transverse scales ($\eta = 8$ times larger), only minor differences are visible, which demonstrates the validity of the scaling model for filamentation. Figure 2(c) illustrates how experimental parameters like input energy, gas pressure, and filament length (defined here as the propagation length over which the intensity on the optical axis exceeds $5 \cdot 10^{13}$ W/cm^2) scale with η.

Figure 2(d) shows a numerically extracted relative scaling error, representing the deviation from perfect scalability for output intensity (dots) and fluence (circles) as a function of ε_{in}. For each pulse energy, the error was calculated by comparing the output intensity (or fluence) to that obtained with 4 times larger pulse energy. While the scaling error is negligibly small for pulse energies well above 1 mJ, thus indicating no fundamental upper scaling limit, a clear deviation from perfect scaling appears for small pulse energies. These deviations can be mainly attributed to avalanche ionization (see Supplement 1).

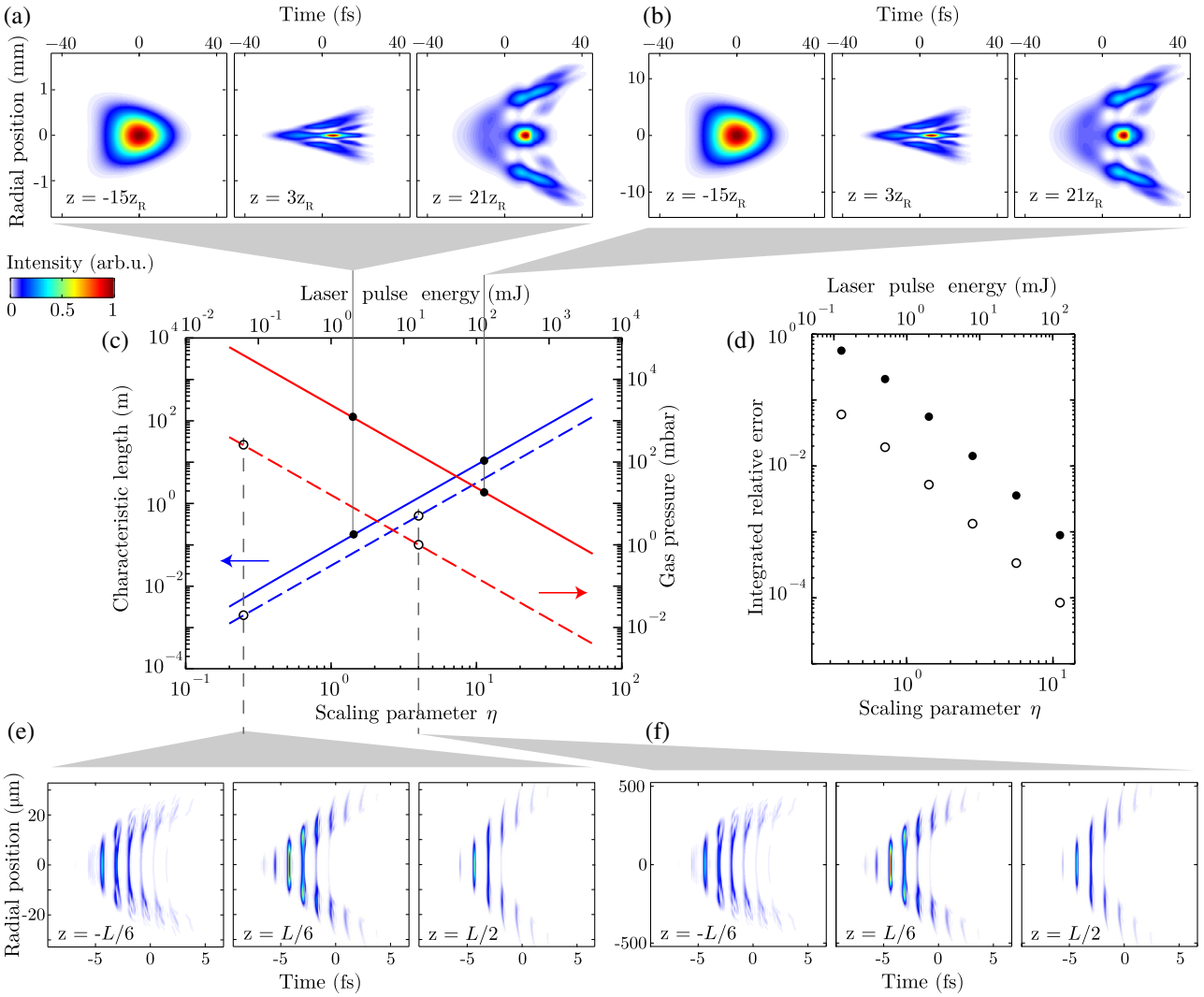

Fig. 2. Scaling filamentation and HHG. (a), (b) Simulated spatiotemporal intensity distributions (normalized individually) in a focused laser beam in Ar for three different positions along the propagation axis and two input parameter sets, scaled according to the presented scaling relations: (a) $\tau = 20$ fs, $\varepsilon_{\text{in}} = 2$ mJ, $p = 1.2$ bar, $W_0 = 40$ μm; (b) $\tau = 20$ fs, $\varepsilon_{\text{in}} = 128$ mJ, $p = 18.75$ mbar, $W_0 = 320$ μm). (e), (f) Simulated spatiotemporal intensity distributions for high-harmonic emission (above 31.5 eV) in Ar [same color scale as used for (a) and (b)] at three positions within the nonlinear medium: (e) $\tau = 10$ fs, $\varepsilon_{\text{in}} = 62.5$ μJ, $p = 256$ mbar, $W_0 = 10.6$ μm, $L = 2$ mm; (f) $\tau = 10$ fs, $\varepsilon_{\text{in}} = 16$ mJ, $p = 1$ mbar, $W_0 = 169.6$ μm, $L = 0.51$ m. For both filamentation and HHG, the longitudinal position is specified with respect to the position of the geometrical focus; in (a) and (b) in units of the respective Rayleigh lengths, and in (e) and (f) in units of the length of the generation medium L. (c) Characteristic length, i.e., filament and gas cell length, respectively (blue, left axis) and gas pressure (red, right axis) as a function of η and ε_{in}. η was arbitrarily set to unity for $\varepsilon_{\text{in}} = 1$ mJ. (d) Integrated relative scaling error for the filament scaling presented in (a) and (b) for intensity (dots) and fluence (circles) (see Supplement 1).

4. SCALING ATTOSECOND PULSE GENERATION

Our second example pertains to HHG, which occurs when intense short laser pulses interact with a gas of atoms or molecules at an intensity of $\sim 10^{14}$ W/cm^2. This process leads to the formation of attosecond light pulses [30], which can be used for pump–probe studies of ultrafast electron dynamics [9]. A major limitation of attosecond science is the low photon flux available [31]. Since the early days, a strong effort has been devoted to optimizing and upscaling HHG [32–35], aiming for an efficient conversion of high laser pulse energies into the extreme ultraviolet (XUV). In spite of this effort, propagation effects and geometrical considerations have limited the useful input laser pulse energy and only a few groups have employed pulse energies exceeding 10 mJ [35–39]. In the opposite direction, progress in laser technology now enables the generation of laser pulses with microjoule energies at megahertz repetition rates [40]. In this regime, macroscopic phase-matching issues have limited the conversion efficiency into the XUV, and only recent attempts point toward a solution of this problem [41,42].

HHG in an extended nonlinear medium can be described in two steps: first, the laser pulse propagates through the nonlinear medium, inducing a polarization $\hat{P}_q = 2d_q\rho$, at multiple odd-order harmonic frequencies, where d_q is the single atom nonlinear dipole moment. Second, the harmonic field $\hat{E}_q$ is generated from the induced polarization. The propagation of $\hat{\mathcal{E}}_q = \hat{E}_q \exp(-i\omega z/c)$, where ω now denotes the harmonic frequency, can be described by equation Eq. (3), with $\hat{\mathcal{P}}_{\text{NL}}$ being replaced by $\hat{\mathcal{P}}_q$. Although both attosecond pulse trains and isolated attosecond pulses are

easily encompassed in our scaling model, for simplicity we concentrate on pulse trains. HHG is known to be very sensitive to macroscopic propagation effects and in particular, to phase matching, i.e., to possible phase offsets between the HHG radiation emitted from different atoms within the nonlinear medium. Such phase offsets can arise due to differences in the phase velocities of the driving laser field and the generated harmonic radiation, as well as due to an intrinsic intensity dependent phase, the so-called dipole phase. As both the fundamental and the harmonic fields follow scale-invariant propagation equations, the phase velocity offset is scalable. Further, the scale invariance of the fundamental field propagation ensures that the intensity distribution and, thus, the dipole phase contribution do not change upon scaling. Furthermore, reabsorption of the generated harmonic radiation in the medium does not change as an increased medium length is compensated by a decreased density. HHG is thus invariant under the scaling transformations. Consequently the harmonic output pulse energy ε_q follows the same scaling as the input pulse energy $\varepsilon_q \to \eta^2 \varepsilon_q$. This implies that the conversion efficiency $\Gamma_q = \varepsilon_q/\varepsilon_{\text{in}}$ is scale-invariant. In other words, the same conversion efficiency can be expected for HHG driven by intense laser pulses with a loose focusing geometry, as well as by much weaker laser pulses with tight focusing geometry, as recently discussed in Refs. [41,42].

We verified the scalability by simulating HHG in Ar, using a simulation code that includes both laser and XUV field propagation effects (see Supplement 1). The dipole response was calculated using the strong field approximation [43]. Figures 2(e) and 2(f) illustrate HHG using 10 fs laser pulses centered at 800 nm. Similar to Figs. 2(a) and 2(b), spatiotemporal intensity maps are displayed that show the evolution of the total field build-up along the nonlinear medium for two parameter sets, differing by $\eta = 16$ (a factor 256 in input energy!). The total field above 31.5 eV (i.e., from the 21st harmonic) is represented. It exhibits a train of ultrashort attosecond pulses. The generation parameters led to strong pulse reshaping effects due to plasma formation, implying that the generation conditions were not optimized for efficient HHG. The high intensity leads to divergent, ring-like emission, except at the rising edge of the laser pulse. Again, an almost perfect scaling behavior can be observed, confirming $\varepsilon_q \to 256\varepsilon_q$.

5. EXPERIMENTAL VERIFICATION

To verify the scaling experimentally, we performed pulse compression experiments via filamentation in gases with 20 fs input pulses (FWHM) centered at 800 nm. The pulse energy was varied in the range of $\varepsilon_{\text{in}} = 0.12 - 2.7$ mJ and spherical mirrors with focal lengths $f = 0.5$–2.5 m were used to focus into an argon-filled tube with a length approximately twice the respective focal length. We scale the pulse energy by a factor of 25, the highest energy being limited by laboratory space constraints. The pulses emerging from the filament were compressed with chirped mirrors and fused silica wedges and characterized using the dispersion-scan technique [44] (see also Supplement 1). Figures 3(a) and 3(b) show temporal intensity as well as spectral amplitude and phase for six different input pulse energies. For the shortest focal lengths (lowest pulse energy), gas pressure and pulse energy were optimized for maximum spectral broadening and good compressibility, while avoiding multiple filamentation. For all other measurement points, focal length and gas pressure were adjusted according to the scaling relations, while the pulse energy was used as a free parameter to optimize the output spectrum, resulting in input pulse energies very close to the scaling prediction. All employed experimental parameters together with fits visualizing the expected scaling trend are displayed in Fig. 3(c). The post-compressed pulse duration and the overall characteristics are very similar for all six cases, indicating very good scalability of all relevant linear and nonlinear propagation processes within the employed parameter range.

Up- (and even down-) scaling HHG has been investigated previously [33,41,42], albeit in a phenomenological way, and in many cases without changing consistently all relevant parameters included in our scaling formalism. To make use of high input energies, loose focusing geometries have been implemented since the early days. Although it was often realized that, in these conditions, the use of long media (and low pressures) led to higher

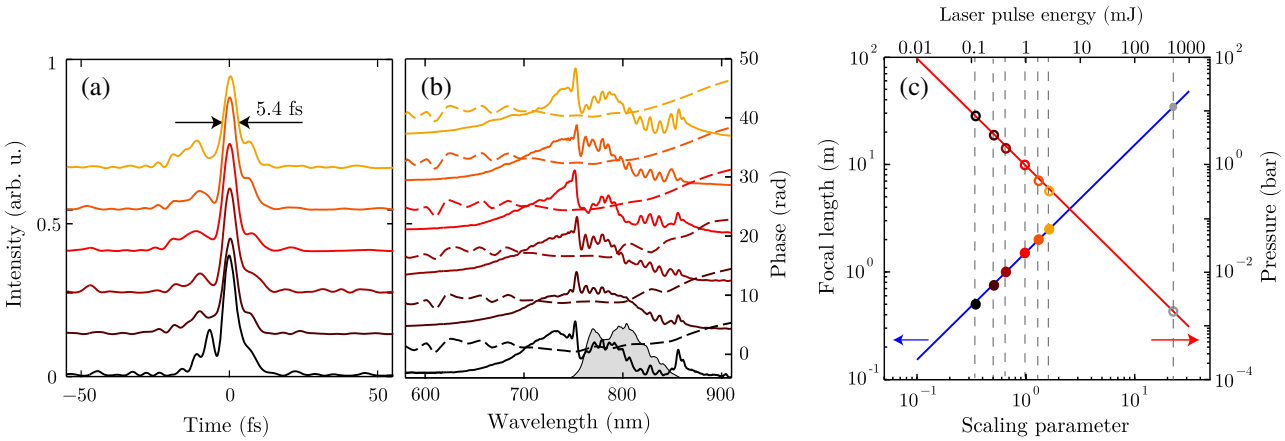

Fig. 3. Experimental filament scaling. (a), (b) Measured temporal intensity profiles as well as spectral power [(b) solid lines] and phase [(b) dashed lines] for six different parameter sets, shown in (c). For better visualization, the plotted datasets are vertically offset from each other. The measurement was performed by selecting the broadband radiation on the optical axis more than a focal length distance behind the filament. For reference, the input spectrum (gray shaded area) is shown in (b). The solid lines in (c) represent fits to the experimental data points, as defined by the presented scaling relations, indicating the expected scaling performance for input laser pulse energies within and beyond the measured parameter range. The gray data points in (c) visualize the extrapolated parameters shown in Table 2.

XUV pulse energies, to our knowledge, no rigorous understanding for this experimental observation has been put forward. In the other direction, tight focusing geometries, necessary for HHG with laser systems with low input energy (down to a few microjoules), have been implemented and found to be detrimental for phase matching, and thus for the conversion efficiency. A recent experiment using a short medium at high pressure [42], however, shows a similar conversion efficiency as with loose focusing, in perfect agreement with our scaling predictions.

6. DISCUSSION AND GENERALITY OF THE SCALING PRINCIPLE

We illustrate the scaling possibilities and experimental challenges for the two phenomena discussed in Table 2. Starting from typical experimental parameters corresponding to $\varepsilon_{\text{in}} \sim 1$ mJ, we apply our scaling relations both for filamentation and HHG up to $\varepsilon_{\text{in}} = 500$ mJ and, for HHG, down to $\varepsilon_{\text{in}} = 10$ μJ, and calculate the expected values for output pulse energy, gas pressure, and focal length. In the case of filamentation, we use the parameters of the experiment presented above and assume that $\varepsilon_{\text{out}} = 0.1\varepsilon_{\text{in}}$ for the central compressed part of the filament. In the case of HHG, we start from values close to those reported in [45] with a conversion efficiency in Ar equal to 10^{-5} (see also [35]). These examples illustrate the feasibility of both up- and down-scaling. Even though long geometries need to be implemented, few-cycle laser pulses and attosecond XUV pulses with unprecedented energies are within reach. Conversely, high gas densities and very tight focusing geometries are required for the efficient generation of attosecond pulses at megahertz repetition rates [42].

Our scaling model does not indicate any fundamental limitation for up-scaling. However, it should be noted that limitations induced because of, for example, nonlinear instabilities may arise when high-power laser systems with reduced laser pulse quality are employed. For down-scaling, several effects leading to deviations from perfect scalability can be identified. First, nonparaxial propagation effects arise at very tight focusing geometries (typically at numerical apertures $\gtrsim 0.3$). Second, the not perfectly linear dependence of $K(\omega, \rho)$ and possibly $\hat{\mathcal{P}}_{\text{NL}}$ on the gas density [see Eq. (3)] as well as the weak dependence of $1/k(\omega, \rho)$ on the density contribute to increasing deviations from perfect scaling. At high ionization levels and high densities, avalanche ionization, a process that critically depends on plasma dynamics and that is not scalable according to our model, can set strict limitations (see Supplement 1). In extreme conditions, the generated plasma can become opaque (for $p \gtrsim 70$ bar at 800 nm and room temperature, assuming a totally singly ionized medium). However, we estimate that these effects do not play a major role within the parameter ranges typically employed, for example, for HHG in gases and for filamentation [see also Fig. 2(d)]. Finally, processes like HHG [46], and, as recent results indicate, even simple ionization phenomena [47], might be affected by the presence of neighboring atoms, especially at high densities. Such many-body interactions could lead to deviations from perfect scaling. Scaling deviations may thus provide an approach to probe such many-body effects, which have so far often been neglected.

Table 2. Extrapolation of Typical Parameters for Filamentation and HHG[a]

	ε_{in}	$\varepsilon_{\text{out}}, \varepsilon_q$	p	f
Filamentation	(mJ)	(mJ)	(mbar)	(m)
Typical	1	0.1	980	1.5
Up-scaled	500	50	1.96	33.5
HHG	(mJ)	(nJ)	(mbar)	(m)
Typical	1.5	15	15	1
Up-scaled	500	5000	0.045	18.3
Down-scaled	0.01	0.1	2300	0.08

[a]The experimentally well-explored regime around $\varepsilon_{\text{in}} \approx 1$ mJ (denoted as typical) is up- and (for HHG) down-scaled. An input pulse length of 20 fs is taken into account for filamentation and 40 fs for HHG, with Ar as the nonlinear medium. The beam diameter (FWHM) before focusing is in both cases ~7 mm.

The presented scaling framework is very general and applies to other processes involving linear or nonlinear electromagnetic wave propagation in gases. The key condition determining if a nonlinear process is scale-invariant is the proportionality $\hat{\mathcal{P}}_{\text{NL}} \propto \rho$. Nonlinear processes that critically depend on plasma dynamics such as avalanche ionization or the acceleration of electrons in relativistic light fields [10] are thus not fully scalable according to our formalism. Furthermore, for processes that make use of the plasma as a source of secondary emission, the frequency dependence of the secondary radiation upon gas density induces a non-negligible departure from $\hat{\mathcal{P}}_{\text{NL}} \propto \rho$ and thus from scale-invariance. Nonlinear interactions that are scalable to a very good approximation include self-focusing, self-phase modulation, and wave mixing, as well as field ionization, plasma defocusing, and processes involving stimulated Raman scattering. Similar scaling principles can also be applied for pulse propagation in waveguides such as hollow capillaries [48].

We expect our results to be of great interest for ultrafast science and beyond as we show how to extend different nonlinear methods to the new parameter regimes provided by today's state-of-the-art femtosecond laser technology. Our findings are currently being applied to the design of an up-scaled, next-generation attosecond source, for the European facility Extreme Light Infrastructure—Attosecond Light Pulse Source (ELI-ALPS).

Funding. European Research Council (ERC); Knut och Alice Wallenberg Foundation; Swedish Research Council; Marie Curie ITN MEDEA; European Union (EU); European Regional Development Fund (GOP-1.1.1-12/B-2012-0001); Hungarian Scientific Research Fund (OTKA project NN107235); ELI-NP (E02/2014); UEFISCDI (PN-II-ID-PCE-2012-4-0342).

Acknowledgment. We thank P. Rudawski, B. Manschwetus, S. Maclot, and P. Johnsson for the experimental verification of the numerical HHG code and their contribution to discussing the scaling of HHG, as well as M. Gisselbrecht for fruitful discussions.

See Supplement 1 for supporting content.

REFERENCES

1. P. Franken, A. Hill, C. Peters, and G. Weinreich, "Generation of optical harmonics," Phys. Rev. Lett. **7**, 118–120 (1961).
2. N. Bloembergen, "From nanosecond to femtosecond science," Rev. Mod. Phys. **71**, S283–S287 (1999).
3. G. Mainfray and G. Manus, "Multiphoton ionization of atoms," Rep. Prog. Phys. **54**, 1333–1372 (1991).
4. H. Conrads and M. Schmidt, "Plasma generation and plasma sources," Plasma Sources Sci. Technol. **9**, 441–454 (2000).

5. M. Nisoli, S. De Silvestri, O. Svelto, R. Szipöcs, K. Ferencz, C. Spielmann, S. Sartania, and F. Krausz, "Compression of high-energy laser pulses below 5 fs," Opt. Lett. **22**, 522–524 (1997).
6. C. Hauri, W. Kornelis, F. Helbing, A. Heinrich, A. Couairon, A. Mysyrowicz, J. Biegert, and U. Keller, "Generation of intense, carrier-envelope phase-locked few-cycle laser pulses through filamentation," Appl. Phys. B **79**, 673–677 (2004).
7. A. Couairon, J. Biegert, C. P. Hauri, W. Kornelis, F. W. Helbing, U. Keller, and A. Mysyrowicz, "Self-compression of ultra-short laser pulses down to one optical cycle by filamentation," J. Mod. Opt. **53**, 75–85 (2006).
8. J. Reintjes, R. Eckardt, C. She, N. Karangelen, R. Elton, and R. Andrews, "Generation of coherent radiation at 53.2 nm by fifth-harmonic conversion," Phys. Rev. Lett. **37**, 1540–1543 (1976).
9. F. Krausz and M. Ivanov, "Attosecond physics," Rev. Mod. Phys. **81**, 163–234 (2009).
10. E. Esarey, C. Schroeder, and W. Leemans, "Physics of laser-driven plasma-based electron accelerators," Rev. Mod. Phys. **81**, 1229–1285 (2009).
11. A. Braun, G. Korn, X. Liu, D. Du, J. Squier, and G. Mourou, "Self-channeling of high-peak-power femtosecond laser pulses in air," Opt. Lett. **20**, 73–75 (1995).
12. P. Russell, "Applied physics: photonic crystal fibers," Science **299**, 358–362 (2003).
13. C. Danson, D. Hillier, N. Hopps, and D. Neely, "Petawatt class lasers worldwide," High Power Laser Sci. Eng. **3**, e3 (2015).
14. J. Limpert, A. Klenke, M. Kienel, S. Breitkopf, T. Eidam, S. Hädrich, C. Jauregui, and A. Tuennermann, "Performance scaling of ultrafast laser systems by coherent addition of femtosecond pulses," IEEE J. Sel. Top. Quantum Electron. **20**, 5 (2014).
15. H. Fattahi, H. G. Barros, M. Gorjan, T. Nubbemeyer, B. Alsaif, C. Y. Teisset, M. Schultze, S. Prinz, M. Haefner, U. M. A. A. L. Vámos, A. Schwarz, O. Pronin, J. Brons, X. T. Geng, G. Arisholm, M. Ciappina, V. S. Yakovlev, D.-E. Kim, A. M. Azzeer, K. N. D. Sutter, Z. Major, T. Metzger, and F. Krausz, "Third-generation femtosecond technology," Optica **1**, 45–63 (2014).
16. A. Husakou and J. Herrmann, "Supercontinuum generation of higher-order solitons by fission in photonic crystal fibers," Phys. Rev. Lett. **87**, 203901 (2001).
17. M. Geissler, G. Tempea, A. Scrinzi, M. Schnürer, F. Krausz, and T. Brabec, "Light propagation in field-ionizing media: Extreme nonlinear optics," Phys. Rev. Lett. **83**, 2930–2933 (1999).
18. A. Couairon and A. Mysyrowicz, "Femtosecond filamentation in transparent media," Phys. Rep. **441**, 47–189 (2007).
19. A. Couairon, M. Franco, A. Mysyrowicz, J. Biegert, and U. Keller, "Pulse self-compression to the single-cycle limit by filamentation in a gas with a pressure gradient," Opt. Lett. **30**, 2657–2659 (2005).
20. J. Marburger, "Self-focusing: theory," Prog. Quantum Electron. **4**, 35–110 (1975).
21. G. Fibich and A. Gaeta, "Critical power for self-focusing in bulk media and in hollow waveguides," Opt. Lett. **25**, 335–337 (2000).
22. M. Mlejnek, M. Kolesik, J. Moloney, and E. Wright, "Optically turbulent femtosecond light guide in air," Phys. Rev. Lett. **83**, 2938–2941 (1999).
23. O. Varela, B. Alonso, I. Sola, J. San Román, A. Zair, C. Méndez, and L. Roso, "Self-compression controlled by the chirp of the input pulse," Opt. Lett. **35**, 3649–3651 (2010).
24. O. Varela, A. Zaïr, J. Román, B. Alonso, I. Sola, C. Prieto, and L. Roso, "Above-millijoule super-continuum generation using polarisation dependent filamentation in atoms and molecules," Opt. Express **17**, 3630–3639 (2009).
25. A. Suda, M. Hatayama, K. Nagasaka, and K. Midorikawa, "Generation of sub-10-fs, 5-mj-optical pulses using a hollow fiber with a pressure gradient," Appl. Phys. Lett. **86**, 11 (2005).
26. C. Fourcade Dutin, A. Dubrouil, S. Petit, E. Mével, E. Constant, and D. Descamps, "Post-compression of high-energy femtosecond pulses using gas ionization," Opt. Lett. **35**, 253–255 (2010).
27. C. L. Arnold, B. Zhou, S. Akturk, S. Chen, A. Couairon, and A. Mysyrowicz, "Pulse compression with planar hollow waveguides: A pathway towards relativistic intensity with table–top lasers," New J. Phys. **12**, 073015 (2010).
28. S. Bohman, A. Suda, M. Kaku, M. Nurhuda, T. Kanai, S. Yamaguchi, and K. Midorikawa, "Generation of 5 fs, 0.5 TW pulses focusable to relativistic intensities at 1 kHz," Opt. Express **16**, 10684–10689 (2008).
29. S. Skupin, G. Stibenz, L. Bergé, F. Lederer, T. Sokollik, M. Schnurer, N. Zhavoronkov, and G. Steinmeyer, "Self-compression by femtosecond pulse filamentation: experiments versus numerical simulations," Phys. Rev. E **74**, 056604 (2006).
30. P. Corkum, N. Burnett, and M. Ivanov, "Subfemtosecond pulses," Opt. Lett. **19**, 1870–1872 (1994).
31. S. Leone, C. McCurdy, J. Burgdörfer, L. Cederbaum, Z. Chang, N. Dudovich, J. Feist, C. Greene, M. Ivanov, R. Kienberger, U. Keller, M. Kling, Z.-H. Loh, T. Pfeifer, A. Pfeiffer, R. Santra, K. Schafer, A. Stolow, U. Thumm, and M. Vrakking, "What will it take to observe processes in 'real time'?" Nat. Photonics **8**, 162–166 (2014).
32. A. L'Huillier, K. J. Schafer, and K. C. Kulander, "Theoretical aspects of intense field harmonic-generation," J. Phys. B **24**, 3315–3341 (1991).
33. E. Takahashi, Y. Nabekawa, T. Otsuka, M. Obara, and K. Midorikawa, "Generation of highly coherent submicrojoule soft x rays by high-order harmonics," Phys. Rev. A **66**, 021802 (2002).
34. T. Popmintchev, M.-C. Chen, D. Popmintchev, P. Arpin, S. Brown, S. Ališauskas, G. Andriukaitis, T. Balčiunas, O. Mücke, A. Pugzlys, A. Baltuška, B. Shim, S. Schrauth, A. Gaeta, C. Hernández-García, L. Plaja, A. Becker, A. Jaron-Becker, M. Murnane, and H. Kapteyn, "Bright coherent ultrahigh harmonics in the keV x-ray regime from mid-infrared femtosecond lasers," Science **336**, 1287–1291 (2012).
35. P. Rudawski, C. M. Heyl, F. Brizuela, J. Schwenke, A. Persson, E. Mansten, R. Rakowski, L. Rading, F. Campi, B. Kim, P. Johnsson, and A. L'Huillier, "A high-flux high-order harmonic source," Rev. Sci. Instrum. **84**, 073103 (2013).
36. E. Takahashi, Y. Nabekawa, and K. Midorikawa, "Generation of 10-μJ coherent extreme-ultraviolet light by use of high-order harmonics," Opt. Lett. **27**, 1920–1922 (2002).
37. J.-F. Hergott, M. Kovacev, H. Merdji, C. Hubert, Y. Mairesse, E. Jean, P. Breger, P. Agostini, B. Carré, and P. Salières, "Extreme-ultraviolet high-order harmonic pulses in the microjoule range," Phys. Rev. A **66**, 021801 (2002).
38. K. Cassou, S. Daboussi, O. Hort, O. Guilbaud, D. Descamps, S. Petit, E. Mével, E. Constant, and S. Kazamias, "Enhanced high harmonic generation driven by high-intensity laser in argon gas-filled hollow core waveguide," Opt. Lett. **39**, 3770–3773 (2014).
39. P. Tzallas, E. Skantzakis, L. Nikolopoulos, G. Tsakiris, and D. Charalambidis, "Extreme-ultraviolet pump-probe studies of one-femtosecond-scale electron dynamics," Nat. Phys. **7**, 781–784 (2011).
40. C.-T. Chiang, A. Blättermann, M. Huth, J. Kirschner, and W. Widdra, "High-order harmonic generation at 4 MHz as a light source for time-of-flight photoemission spectroscopy," Appl. Phys. Lett. **101**, 071116 (2012).
41. C. M. Heyl, J. Güdde, A. L'Huillier, and U. Höfer, "High-order harmonic generation with μJ laser pulses at high repetition rates," J. Phys. B **45**, 074020 (2012).
42. J. Rothhardt, M. Krebs, S. Hädrich, S. Demmler, J. Limpert, and A. Tünnermann, "Absorption-limited and phase-matched high harmonic generation in the tight focusing regime," New J. Phys. **16**, 033022 (2014).
43. M. Lewenstein, P. Balcou, M. Ivanov, A. L'Huillier, and P. Corkum, "Theory of high-harmonic generation by low-frequency laser fields," Phys. Rev. A **49**, 2117–2132 (1994).
44. M. Miranda, T. Fordell, C. Arnold, A. L'Huillier, and H. Crespo, "Simultaneous compression and characterization of ultrashort laser pulses using chirped mirrors and glass wedges," Opt. Express **20**, 688–697 (2012).
45. E. Constant, D. Garzella, P. Breger, E. Mével, C. Dorrer, C. L. Blanc, F. Salin, and P. Agostini, "Optimizing high harmonic generation in absorbing gases: model and experiment," Phys. Rev. Lett. **82**, 1668–1671 (1999).
46. V. Strelkov, V. Platonenko, and A. Becker, "High-harmonic generation in a dense medium," Phys. Rev. A **71**, 053808 (2005).
47. K. Schuh, J. Hader, J. V. Moloney, and S. W. Koch, "Influence of optical and interaction-induced dephasing effects on the short-pulse ionization of atomic gases," J. Opt. Soc. Am. B **32**, 1442–1449 (2015).
48. F. Böhle, M. Kretschmar, A. Jullien, M. Kovacs, M. Miranda, R. Romero, H. Crespo, U. Morgner, P. Simon, R. Lopez-Martens, and T. Nagy, "Compression of CEP-stable multi-mJ laser pulses down to 4 fs in long hollow fibers," Laser Phys. Lett. **11**, 095401 (2014).